



# Hydrogenation of Aliphatic Nitriles to Primary Amines over a Bimetallic Catalyst $\text{Ni}_{25.38}\text{Co}_{18.21}/\text{MgO}-0.75\text{Al}_2\text{O}_3$ Under Atmospheric Pressure

Dongxu Shi<sup>1</sup> · He Zhu<sup>1</sup> · Yaping Han<sup>1</sup> · Yuecheng Zhang<sup>1,3</sup> · Jiquan Zhao<sup>1,2</sup>

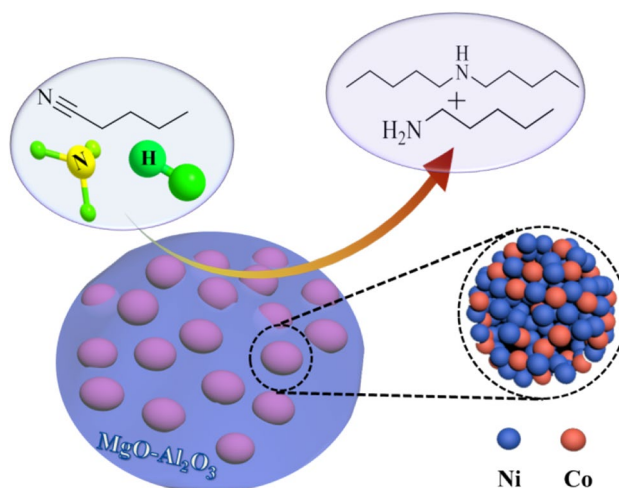
Received: 23 November 2020 / Accepted: 4 January 2021

© The Author(s), under exclusive licence to Springer Science+Business Media, LLC part of Springer Nature 2021

## Abstract

A mixed oxide supported bimetallic catalyst  $\text{Ni}_{25.38}\text{Co}_{18.21}/\text{MgO}-0.75\text{Al}_2\text{O}_3$  was readily prepared and found to be efficient in the hydrogenation of valeronitrile (VN) to amylamine (AA) under atmospheric pressure. Under the optimal conditions:  $\text{H}_2$  to VN molar ratio of 4:1,  $\text{NH}_3$  to VN molar ratio of 3:1, reaction temperature of 130 °C and residence time of 5 s, the conversion of VN reached 100% with a AA yield of 70.8%, and a diamylamine (DAA) yield of 25.9%. This catalyst was also active in the hydrogenation of other low carbon aliphatic nitriles to their corresponding primary amines. The characterization results revealed that the catalyst had the properties of large surface area, uniform and fine dispersion of metal particles in the form of Ni/Co alloy with synergy effect between the two metals, which endowed the catalyst with good catalytic performances in the hydrogenation reaction of aliphatic nitriles.

## Graphic Abstract



**Keywords** Ni/Co bimetallic catalyst · Nitrile hydrogenation · Valeronitrile · Amylamine · Mixed  $\text{MgO}-\text{Al}_2\text{O}_3$  support

**Supplementary Information** The online version contains supplementary material available at <https://doi.org/10.1007/s10562-021-03532-9>.

✉ Yuecheng Zhang  
yczhang@hebut.edu.cn

✉ Jiquan Zhao  
zhaojq@hebut.edu.cn

Extended author information available on the last page of the article

## 1 Introduction

Amines are widely used in the production of agrochemicals, pharmaceuticals, dyestuffs, polymers, pigments, plasticizing agents, and emulsifiers [1–3]. Among which, the primary amines are the most versatile intermediates or precursors in industrial synthesis due to their ease of functionalization.

Accordingly, the selective synthesis of primary amines is of significant importance. Several protocols have been developed to synthesize primary amines, such as reductive amination of carbonyl compounds [4, 5], nucleophilic substitution of ammonia on haloalkanes [6], direct amination of alcohols with ammonia [7–9], and hydrogenation of nitro compounds [10–12], nitriles [13], and amides [14]. Among all the methods, the direct amination of alcohols with ammonia over heterogeneous catalysts is the most recommended protocol for commercial production of amines because of ready availability and low cost of alcohols compared to carbonyl compounds as raw materials in general. Moreover, water is the only by-product in the process in principle, which is consistent with the concept of green chemistry. However, most of the developed heterogeneous processes were not compatible to the direct amination of primary aliphatic alcohols to the terminal primary amines [15]. Therefore, the selective hydrogenation of aliphatic nitriles to terminal primary amines might be a good alternative, because aliphatic nitriles can be obtained from primary alcohols and ammonia via dehydrogenation–amination over heterogeneous catalysts, being a green chemical process [16–20]. Nevertheless, the selective hydrogenation of aliphatic nitriles to the terminal primary amines is a complicated process due to the inevitable side reactions [13]. As shown in Scheme 1, the hydrogenation of nitrile **1** generates an imine intermediate **2**. Due to the high reactivity of **2**, a set of consecutive and parallel reactions takes place and leads to a mixture of primary **3**, secondary **5** and tertiary amines **7** via imine intermediates **4** and **6**. The key issue in the hydrogenation of nitriles to primary amines is to prevent the formation of secondary and tertiary amines. Generally, the introduction of ammonia is often used to increase the selectivity of the primary amine [13].

Both homogeneous and heterogeneous catalysts have been developed for the hydrogenation of nitriles to primary amines [13, 21–31], and heterogeneous catalysts are more suitable for the production of bulk primary amines. Up till now, the industrial production of terminal primary amines

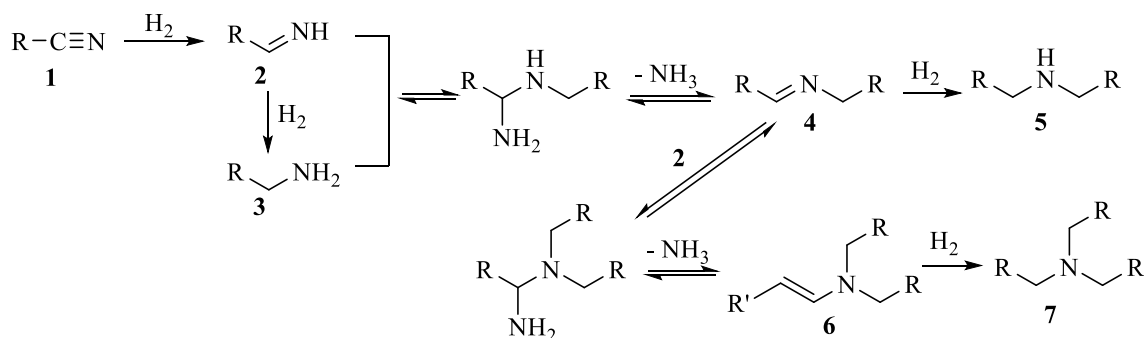
from catalytic hydrogenation of nitriles is generally realized in the liquid phase over heterogeneous catalysts such as Raney® nickel or cobalt [13]. It is well known that the hydrogenation in gas phase has the advantages of easy operation, safety, and stable product quality. However, only a few catalysts especially the non-noble metal based catalysts have been found to be efficient in the gas phase hydrogenation of nitriles to primary amines [27–29]. Among the catalysts, a series of Co–Ni bimetallic catalysts derived from layered double hydroxides (LDHs) with a hydrotalcite-like structure and containing  $\text{Ni}^{2+}$ ,  $\text{Co}^{2+}$ ,  $\text{Mg}^{2+}$ ,  $\text{Al}^{3+}$  showed good performances in the hydrogenation of acetonitrile to ethylamine in gas phase [29]. However, the preparation processes of these catalysts were too complicated. Therefore, it is of great importance to develop a catalyst with characters of high activity, low cost, and ease of preparation for the selective gas phase hydrogenation of aliphatic nitriles to the corresponding primary aliphatic amines.

Herein, we report the preparation, characterization, and catalysis of a bimetallic catalyst  $\text{Ni}_{25.38}\text{Co}_{18.21}/\text{MgO}-0.75\text{Al}_2\text{O}_3$  in the hydrogenation of aliphatic nitriles to terminal primary aliphatic amines. The catalyst showed good catalytic performances in the gas phase hydrogenation of several aliphatic nitriles in a fixed bed reactor under atmospheric pressure.

## 2 Experimental

### 2.1 Catalyst Preparation

All reagents were analytical grade and used as received without further purification. Metal nitrates and reagents for catalyst preparation were purchased from Tianjin Keruisi Chemical Reagent Cooperation. Nitriles and standard amines were provided by Tianjin Hengshan Chemical Technology Cooperation. Valeronitrile (VN) with a purity higher than 99% was prepared in our laboratory from amyl alcohol over a catalyst  $\text{FeZn}/\gamma\text{-Al}_2\text{O}_3$  in a fixed bed reactor.



**Scheme 1** Reaction pathways in the catalytic hydrogenation of nitriles

The designed catalysts are denoted as  $\text{Ni}_x\text{Co}_y/\text{mMgO}-\text{nAl}_2\text{O}_3$ , where the subscripts  $x$  and  $y$  are respective mass contents of nickel and cobalt in a bimetallic catalyst;  $m:n$  is the molar ratio of  $\text{MgO}$  to  $\text{Al}_2\text{O}_3$ , and  $m$  is 0 or 1. If  $m$  or  $n$  is 1,  $1\text{MgO}$  or  $1\text{Al}_2\text{O}_3$  is directly written as  $\text{MgO}$  or  $\text{Al}_2\text{O}_3$ . The catalysts were obtained from their precursors by in situ calcination in a fixed bed reactor, and the catalyst precursors were prepared by a coprecipitation method as illustrated by the following examples.

- (1) The precursor of mixed oxide supported bimetallic catalyst  $\text{Ni}_{25.38}\text{Co}_{18.21}/\text{MgO}-0.75\text{Al}_2\text{O}_3$ :

Into 200 mL of deionized water in a beaker were added 20.36 g of  $\text{Ni}(\text{NO}_3)_2 \cdot 6\text{H}_2\text{O}$ , 14.55 g of  $\text{Co}(\text{NO}_3)_2 \cdot 6\text{H}_2\text{O}$ , 20.51 g of  $\text{Mg}(\text{NO}_3)_2 \cdot 6\text{H}_2\text{O}$  and 45.02 g of  $\text{Al}(\text{NO}_3)_3 \cdot 9\text{H}_2\text{O}$  successively. The mixture was stirred at room temperature for a while to give a clean solution **A**. Next, 12.00 g of  $\text{NaOH}$  and 15.90 g of  $\text{Na}_2\text{CO}_3$  were dissolved in 200 mL of deionized water in another beaker to obtain a solution **B**. The solution **B** was added dropwise into the solution **A** under stirring until the pH of the mixture reached 9.0. The mixture was stirred strongly for another 2 h, then, the solid was collected by centrifugation, and thoroughly washed with deionized water under stirring until the pH of the supernatant reached 7.0. The solid was separated by vacuum filtration and dried in an oven at  $80^\circ\text{C}$  for 12 h. The dried solid was ground in a ball crusher to give a powder with a particle size  $< 200$  mesh. Into a beaker, 30.0 g of the resulted powder, 0.1 g of sesbania powder and an appropriate amount of deionized water were added successively. The mixture was kneaded in a kneader thoroughly to give a paste which was processed in an extruder to obtain extrudates with a diameter of 2 mm. The extrudates were dried in air at room temperature for 12 h, and then moved into an oven to dry at  $80^\circ\text{C}$  for 10 h. The dried extrudates were cut into columns with a length of 2 mm to yield the precursor of catalyst  $\text{Ni}_{25.38}\text{Co}_{18.21}/\text{MgO}-0.75\text{Al}_2\text{O}_3$ .

- (2) The precursor of mixed oxide supported monometallic catalyst  $\text{Ni}_{43.55}/\text{MgO}-0.5\text{Al}_2\text{O}_3$ : See Supporting Information.
- (3) The precursor of mono oxide supported monometallic catalyst  $\text{Ni}_{46.63}/\text{MgO}$ : See Supporting Information.

## 2.2 Characterization of Catalysts

The X-ray diffraction (XRD) patterns of the samples were taken on a Bruker D8 X-ray diffractometer with Ni-filtered  $\text{Cu K}\alpha$  radiation (150 mA, 40 kV) in the  $2\theta$  range of  $5^\circ$ – $90^\circ$ . The spectra of X-ray photoelectron spectroscopy (XPS) were recorded using a Thermo ESCALAB 250XI spectrometer with monochromatic  $\text{Mg K}\alpha$  radiation.  $\text{N}_2$

adsorption–desorption was performed on a Micromeritics ASAP 2020 at 77 K to determine the surface area, total pore volume and pore size distribution of the samples. The specific surface areas and pore sizes of the samples were calculated by Brunauer–Emmett–Teller (BET) method. The transmission electron micrographs (TEM) images were taken on a JEM 2100F instrument at accelerating voltage of 200 kV. The samples were dispersed ultrasonically in ethanol to prepare the specimens for TEM analysis, where a drop of the suspension was evaporated on a lacey-carbon/copper grid.

## 2.3 Catalytic Test

The catalytic hydrogenation of valeronitrile (VN) to amylamine (AA) was conducted in a fixed-bed reactor with an inner diameter of 20 mm and a length of 1000 mm installed in an electric furnace. The furnace consists of four heating zones equipped with four temperature controllers. Before catalytic test, the thermocouple, mass flow controller and advection pump in the equipment system were calibrated precisely, and the gas tightness of the device was checked carefully.

In a typical process, 25 mL of the catalyst precursor was loaded into the center a fix-bed reactor, while the bottom and top of the reactor were filled with inert Pyrex glass chips. The temperature of the catalyst bed was increased to  $600^\circ\text{C}$  with a ramp rate of  $5^\circ\text{C}/\text{min}$  under  $\text{N}_2$  atmosphere. Thus, the catalyst precursor was converted to the catalyst. Then,  $\text{H}_2$  was introduced at rate of 100 mL/min to reduce the catalyst for 2 h. After the reduction, the temperature was adjusted to the required temperature under a nitrogen atmosphere. The controlled flows of VN, ammonia and hydrogen were introduced separately into a vaporizer where the three reactants were preheated, vaporized and mixed thoroughly. Then the mixed gaseous reactants were fed into the catalyst bed under atmospheric pressure. The reaction mixture was passed through a condenser, and collected in a flask. The collected reaction mixture was subjected to GC analysis.

## 2.4 Product Analysis

Reaction mixture was analyzed by a gas chromatography equipped with a SE-54 capillary column ( $30\text{ m} \times 0.32\text{ mm} \times 0.50\ \mu\text{m}$ ) using the internal standard method. The content of each liquid product was calculated using calibration curves, with butanol as an internal standard. The GC temperature program was set to  $80^\circ\text{C}$  for 1 min,  $3^\circ\text{C}/\text{min}$  up to  $110^\circ\text{C}$  and  $30^\circ\text{C}/\text{min}$  up to  $250^\circ\text{C}$ .

$$\text{VN conversion (\%)} = \frac{\text{moles of VN reacted}}{\text{moles of VN fed}} \times 100\%$$

$$\text{AA selectivity (\%)} = \frac{\text{moles of VN consumed to produce AA}}{\text{moles of VN reacted}} \times 100\%$$

$$\text{DAA selectivity (\%)} = 2 \times \frac{\text{moles of VN consumed to produce AA}}{\text{moles of VN reacted}} \times 100\%$$

$$\text{Yield (\%)} = \text{conversion} \times \text{selectivity} \times 100\%$$

### 3 Results and Discussion

#### 3.1 Screen of the Catalysts

It was reported that oxide supported nickel catalysts were active in the hydrogenation of nitriles to amines either in gas phase or liquid phase [24, 29]. Besides, the oxide supports such as Al<sub>2</sub>O<sub>3</sub> and MgO had strong effects on the performances of the catalysts [32, 33]. Therefore, three oxide supported monometallic nickel catalysts Ni<sub>46.63</sub>/MgO, Ni<sub>40.85</sub>/Al<sub>2</sub>O<sub>3</sub>, and Ni<sub>43.55</sub>/MgO–0.5Al<sub>2</sub>O<sub>3</sub> were firstly prepared, and evaluated in the hydrogenation of VN to AA under atmospheric pressure in the presence of ammonia in a fixed bed reactor. As shown in Table 1 (Entries 1–4), the catalyst Ni<sub>46.63</sub>/MgO gave the lowest VN conversion of 58.2%, but the highest AA selectivity of 64.4%. Compared to Ni<sub>46.63</sub>/MgO, Ni<sub>40.85</sub>/Al<sub>2</sub>O<sub>3</sub> exhibited a good VN conversion of 72.3%, but a poor AA selectivity of 55.3%. The mixed oxide supported catalyst Ni<sub>43.55</sub>/MgO–0.5Al<sub>2</sub>O<sub>3</sub> showed the best result in view of the yield of AA as high as 45.1%. These results indicated that the catalytic performances of the catalysts were related to the properties of the supports [28, 29, 34–36]. For comparison, a mixed oxide supported cobalt catalyst Co<sub>43.65</sub>/MgO–0.5Al<sub>2</sub>O<sub>3</sub> was also prepared, but very poor results were received over this catalyst, indicating the necessity of nickel in the catalysts.

Generally, bimetallic catalysts exhibited good catalytic performances compared to monometallic ones in the hydrogenation of nitriles [37–40]. Next, a series of Ni–Co bimetallic catalysts with different nickel to cobalt molar ratios but a constant total metal molar percent were prepared, and evaluated in the hydrogenation of VN under the same reaction conditions. As shown in the Table 1 (Entries 5–9), the catalyst Ni<sub>25.38</sub>Co<sub>18.21</sub>/MgO–0.5Al<sub>2</sub>O<sub>3</sub>, in which the nickel to cobalt molar ratio is 1.4:1, exhibited the best results among all the tested bimetallic catalysts, and also performed better than the monometallic catalyst Ni<sub>43.55</sub>/MgO–0.5Al<sub>2</sub>O<sub>3</sub> in view of both the conversion of VN and the yield of AA. Either increase or decrease in nickel to cobalt molar ratio led to the reduction of both the conversion of VN and the yield of AA.

After determining the molar ratio of nickel to cobalt, the MgO to Al<sub>2</sub>O<sub>3</sub> molar ratio was then screened, too. Several catalysts were prepared with different MgO to Al<sub>2</sub>O<sub>3</sub> ratios but constant contents of nickel and cobalt. As shown in Table 1 (Entries 6, 10–13), no big difference was observed in either the conversion of VN or the yield of AA in the screened MgO to Al<sub>2</sub>O<sub>3</sub> molar ratio range of 1:0.41–1: 0.75, which indicated that the MgO to Al<sub>2</sub>O<sub>3</sub> molar ratio had no major effects on the catalysis of the catalysts. Taking into account a slightly higher AA yield of 50.8% received in the MgO to Al<sub>2</sub>O<sub>3</sub> molar ratio of 1: 0.75, as well as the lower cost of Al<sub>2</sub>O<sub>3</sub> than MgO, Ni<sub>25.38</sub>Co<sub>18.21</sub>/MgO–0.75Al<sub>2</sub>O<sub>3</sub> was finally chosen as the best catalyst.

#### 3.2 Optimization of Reaction Conditions

After the catalyst Ni<sub>25.38</sub>Co<sub>18.21</sub>/MgO–0.75Al<sub>2</sub>O<sub>3</sub> was chosen, the reaction parameters affecting the hydrogenation

**Table 1** Catalysis of various oxide supported nickel catalysts in the hydrogenation of VN

| Entry | Catalyst  | Ni:Co<br>(molar ratio) | MgO:Al <sub>2</sub> O <sub>3</sub><br>(molar ratio) | Con.<br>(%) | AA<br>Sel. (%) | AA<br>yield (%) | DAA<br>Sel. (%) |
|-------|---|------------------------|---|-------------|----------------|-----------------|-----------------|
| 1     | Ni <sub>46.63</sub> /MgO  | –                      | –   | 58.2        | 64.4           | 37.5            | 22.5            |
| 2     | Ni <sub>40.85</sub> /Al <sub>2</sub> O <sub>3</sub>                             | –                      | –   | 72.3        | 55.3           | 40.0            | 26.1            |
| 3     | Ni <sub>43.55</sub> /MgO–0.5Al <sub>2</sub> O <sub>3</sub>                      | –                      | 1:0.5   | 78.0        | 57.9           | 45.1            | 26.4            |
| 4     | Co <sub>43.65</sub> /MgO–0.5Al <sub>2</sub> O <sub>3</sub>                      | –                      | 1:0.5   | 4.3         | 16.4           | 0.7             | 13.7            |
| 5     | Ni <sub>29.00</sub> Co <sub>14.57</sub> /MgO–0.5Al <sub>2</sub> O <sub>3</sub>  | 2:1                    | 1:0.5   | 82.3        | 49.4           | 40.7            | 40.7            |
| 6     | Ni <sub>25.38</sub> Co <sub>18.21</sub> /MgO–0.5Al <sub>2</sub> O <sub>3</sub>  | 1.4:1                  | 1:0.5   | 84.5        | 56.9           | 48.1            | 33.4            |
| 7     | Ni <sub>22.00</sub> Co <sub>22.00</sub> /MgO–0.5Al <sub>2</sub> O <sub>3</sub>  | 1:1                    | 1:0.5   | 81.3        | 58.0           | 47.2            | 29.6            |
| 8     | Ni <sub>18.13</sub> Co <sub>25.49</sub> /MgO–0.5Al <sub>2</sub> O <sub>3</sub>  | 0.71:1                 | 1:0.5   | 74.5        | 53.4           | 39.8            | 26.9            |
| 9     | Ni <sub>14.92</sub> Co <sub>28.88</sub> /MgO–0.5Al <sub>2</sub> O <sub>3</sub>  | 0.5:1                  | 1:0.5   | 69.2        | 49.5           | 34.2            | 26.5            |
| 10    | Ni <sub>25.38</sub> Co <sub>18.21</sub> /MgO–0.33Al <sub>2</sub> O <sub>3</sub> | 1.4:1                  | 1:0.33  | 79.6        | 54.8           | 43.6            | 31.5            |
| 11    | Ni <sub>25.38</sub> Co <sub>18.21</sub> /MgO–0.41Al <sub>2</sub> O <sub>3</sub> | 1.4:1                  | 1:0.41  | 84.4        | 56.0           | 47.3            | 32.4            |
| 12    | Ni <sub>25.38</sub> Co <sub>18.21</sub> /MgO–0.61Al <sub>2</sub> O <sub>3</sub> | 1.4:1                  | 1:0.61  | 85.4        | 58.7           | 50.1            | 30.8            |
| 13    | Ni <sub>25.38</sub> Co <sub>18.21</sub> /MgO–0.75Al <sub>2</sub> O <sub>3</sub> | 1.4:1                  | 1:0.75  | 86.6        | 58.7           | 50.8            | 30.1            |

Reaction conditions: temperature 130 °C, NH<sub>3</sub> to VN molar ratio=4:1, H<sub>2</sub> to VN molar ratio=2:1, residence time 4.5 s, time on stream 6–8 h, atmospheric pressure

of VN were studied systematically to improve the yield of AA. First, the effect of reaction temperature on the reaction was investigated under atmospheric pressure, residence time of 4.5 s,  $\text{NH}_3$  to VN molar ratio of 4:1, and  $\text{H}_2$  to VN molar ratio of 2:1. As shown in Fig. 1, the VN conversion increased from 63.9 to 86.6% with increase in reaction temperature from 110 to 130 °C, then changed slightly with a further increase in reaction temperature. The AA yield also increased with temperature initially and reached its maximum of 50.9% at 130 °C, and then turned to slight decrease with a further increase in reaction temperature due to the formation of more DAA. Besides, the total yield of AA and DAA was 77.0% at 130 °C.

Next, the effect of the molar ratio of  $\text{H}_2$  to VN on the reaction was studied in the range of 1.5:1–6:1 at 130 °C under atmospheric pressure, residence time of 4.5 s, and molar ratio of  $\text{NH}_3$  to VN of 4:1. As shown in Fig. 2, both the conversion of VN and the yield of AA increased with increase in  $\text{H}_2$  to VN molar ratio from 1.5:1 to 4:1, and then remained almost constant. When the molar ratio of  $\text{H}_2$  to VN was equal to or higher than 4:1, the conversion of VN was always close to 100%, and the yield of AA was 65.7%. Meanwhile, the total yield of AA and DAA reached 89.4%. The results indicated that a high fraction of hydrogen in the gaseous mixture favored the transformation of VN to amines.

Then, the effect of the molar ratio of  $\text{NH}_3$  to VN on the reaction was investigated in the range of 2:1–6:1 at 130 °C under atmospheric pressure, residence time of 4.5 s, and  $\text{H}_2$  to VN molar ratio of 4:1. As shown in Fig. 3, the VN conversion was always close to 100% in the screened molar ratio range of  $\text{NH}_3$  to VN. However, the yield of AA increased

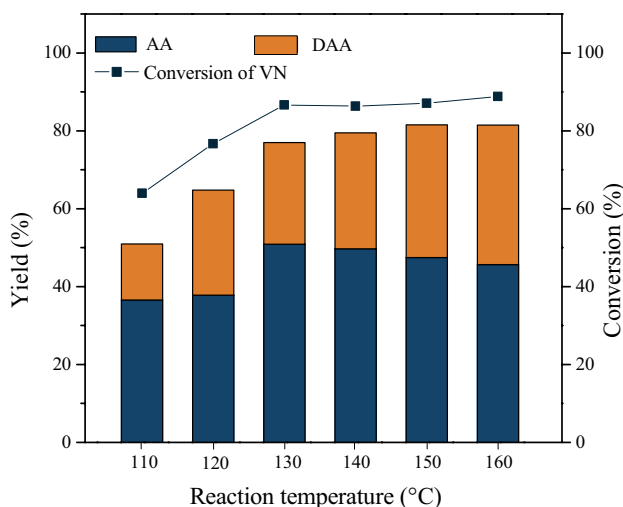


**Fig. 1** Effect of the temperature on the catalysis of  $\text{Ni}_{25.38}\text{Co}_{18.21}/\text{MgO}-0.75\text{Al}_2\text{O}_3$ . Reaction conditions:  $\text{NH}_3$  to VN molar ratio=4:1,  $\text{H}_2$  to VN molar ratio of=2:1, atmospheric pressure, residence time 4.5 s, time on stream 6–8 h

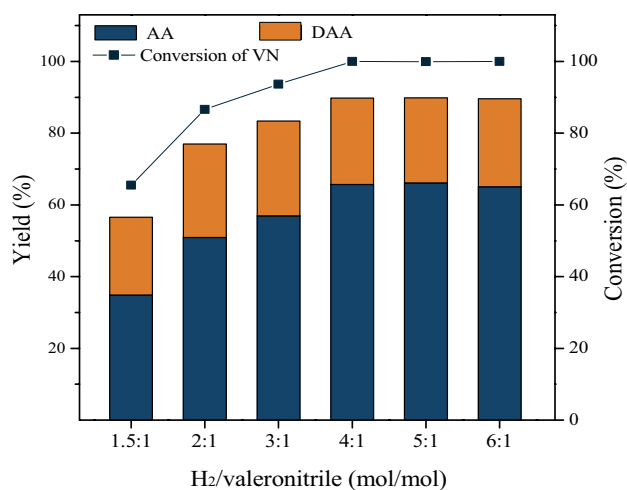


**Fig. 2** Effect of  $\text{H}_2$  to VN molar ratio on the catalysis of  $\text{Ni}_{25.38}\text{Co}_{18.21}/\text{MgO}-0.75\text{Al}_2\text{O}_3$ . Reaction conditions: ammonia to VN molar ratio=4:1, temperature 130 °C, residence time 4.5 s, atmospheric pressure, time on stream 6–8 h

with increase in  $\text{NH}_3$  to VN molar ratio from 2:1 to 3:1, and reached its maximum of 68.7% at the molar ratio of 3:1. Instead, a further increase in  $\text{NH}_3$  to VN molar ratio led to the decrease of the yield of AA. Meanwhile, the total yield of AA and DAA reached its maximum of 94.0% at the  $\text{NH}_3$  to VN molar ratio of 2:1. As shown in Scheme 1, dialkylimine (4) undergoes transimination with  $\text{NH}_3$  to give alkylimine (2) and alkylamine (3). Ammonia is in favor of a shift of the transimination equilibrium to the side of the primary imine and amine [41]. Therefore, an appropriate amount of ammonia enhanced the selectivity of primary amine in the

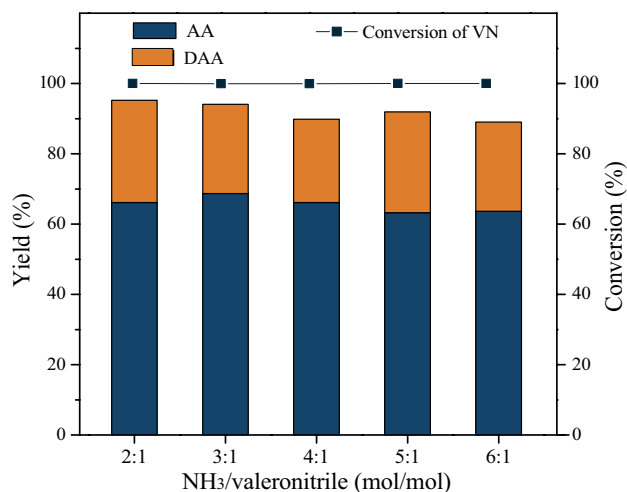


**Fig. 3** Effect of  $\text{NH}_3$  to VN molar ratio on the catalysis of  $\text{Ni}_{25.38}\text{Co}_{18.21}/\text{MgO}-0.75\text{Al}_2\text{O}_3$ . Reaction conditions: temperature 130 °C,  $\text{H}_2$  to VN molar ratio=4:1, time on stream 6–8 h, atmospheric pressure, residence time 4.5 s

hydrogenation of VN. However, much excessive ammonia could dilute the concentration of hydrogen, which deteriorated the hydrogenation of alkyimine to AA.

Residence time is another important parameter affecting a gas phase reaction in a fixed bed reactor, therefore, its effect on the hydrogenation of VN over the catalyst  $\text{Ni}_{25.38}\text{Co}_{18.21}/\text{MgO}-0.75\text{Al}_2\text{O}_3$  was studied at 130 °C under atmospheric pressure,  $\text{H}_2$  to VN molar ratio of 4:1, and  $\text{NH}_3$  to VN molar ratio of 3:1. As shown in Fig. 4, both the conversion of VN and the yield of AA increased with increase in residence time from 3.5 to 5.0 s, and reached their maxima of 100% and 70.8% at the residence time of 5.0 s, respectively. Meanwhile, the total yield of AA and DAA reached its maximum of 96.7%. With a further increase in residence time of longer than 5.0 s, the conversion of VN maintained 100%, but the yield of AA decreased. Meanwhile, the yield of DAA increased. The results indicated that a longer residence time led to the transformation of more AA to DAA.

Based on the above experimental results, the optimal parameters for the hydrogenation of VN to AA were obtained, which are atmospheric pressure,  $\text{H}_2$  to VN molar ratio of 4:1,  $\text{NH}_3$  to VN molar ratio of 3:1, reaction temperature of 130 °C, and residence time of 5 s. Under the optimal conditions, the conversion of VN reached 100% with an AA yield of 70.8%, and a total yield of AA and DAA of 96.7%.

### 3.3 Hydrogenation of Other Aliphatic Nitriles

Under the optimal conditions of VN hydrogenation, the catalyst  $\text{Ni}_{25.38}\text{Co}_{18.21}/\text{MgO}-0.75\text{Al}_2\text{O}_3$  was then applied to the hydrogenation of several other aliphatic nitriles. As shown in Table S1 the catalyst showed good performances in the

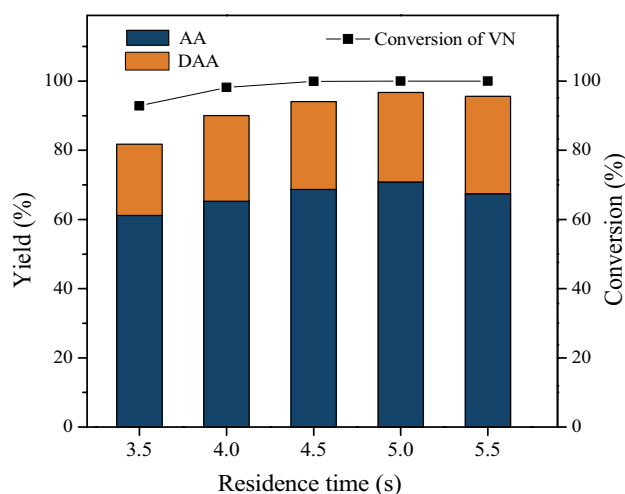


**Fig. 4** Effect of the residence time on the catalysis of  $\text{Ni}_{25.38}\text{Co}_{18.21}/\text{MgO}-0.75\text{Al}_2\text{O}_3$ . Reaction conditions:  $\text{NH}_3$  to VN molar ratio=3:1, atmospheric pressure,  $\text{H}_2$  to VN molar ratio=4:1, temperature 130 °C, reaction time 6–8 h

hydrogenation of  $\text{C}_6$ – $\text{C}_8$  aliphatic nitriles. In these cases the conversions of three nitriles were higher than 81%, and the yields of the corresponding primary amines were 62.5%, 58.0% and 60.1%, respectively. However, the catalyst performed poorly in the hydrogenation of laurionitrile. In this case the conversion of laurionitrile was only 61.3% with a laurylamine yield of 47.3%. It was noted that the longer the carbon chain of aliphatic nitrile, the lower the conversion of the substrate, as well as the yield of the primary amine. The results could be ascribed to the big inner diffusion resistance of long carbon chain substrates in the catalyst. The results will be improved if the hydrogenation reaction is conducted under the optimal conditions of the specific substrate. It is expected that the catalyst  $\text{Ni}_{25.38}\text{Co}_{18.21}/\text{MgO}-0.75\text{Al}_2\text{O}_3$  will have wide applications in the hydrogenation of aliphatic nitriles to primary amines.

### 3.4 Lifetime and Regeneration of the Catalyst

The lifetime and the regeneration of  $\text{Ni}_{25.38}\text{Co}_{18.21}/\text{MgO}-0.75\text{Al}_2\text{O}_3$  were then studied in the hydrogenation of VN under the optimal reactions. As shown in Fig. 5, the conversion of VN was always close to 100% in the first 30 h of the catalyst on stream, and then decreased slightly from 30 to 60 h. Meanwhile, the yield of AA decreased slowly, and dropped from 70.8 to 66.5% from 5 to 60 h of the catalyst on stream. The used catalyst was regenerated by on-line hydrogenation at 600 °C for 2 h, and then tested again on the reaction. As shown in Fig. 5, both the conversion of VN and the yield of AA over the regenerated catalyst were close to those over the fresh catalyst. The results indicated that the catalyst was stable on stream and could be easily regenerated.

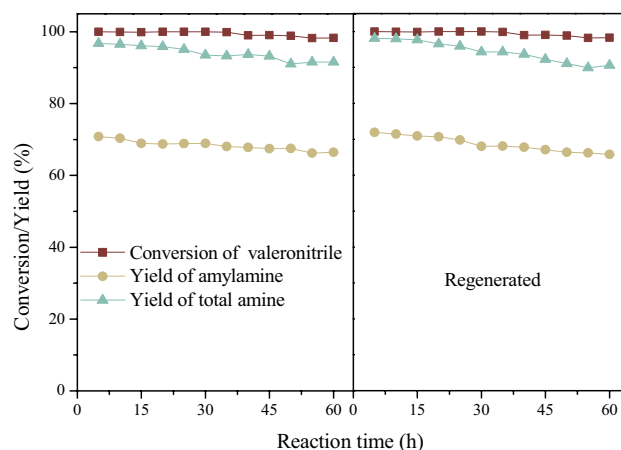


**Fig. 5** Catalytic results of the fresh and the used  $\text{Ni}_{25.38}\text{Co}_{18.21}/\text{MgO}-0.75\text{Al}_2\text{O}_3$  with time on stream. Reaction conditions:  $\text{NH}_3$  to VN molar ratio=3:1,  $\text{H}_2$  to VN molar ratio=4:1, atmospheric pressure temperature 130 °C, residence time 5 s

### 3.5 Catalyst Characterization

The reduced catalysts were characterized by XRD, XPS,  $N_2$  adsorption and desorption, and TEM to reveal the relationship between catalytic performance and microstructure. The XRD patterns of the samples of the reduced  $Ni_{46.63}/MgO$ ,  $Ni_{40.85}/Al_2O_3$ ,  $Ni_{43.55}/MgO-0.5Al_2O_3$ ,  $Ni_{25.38}Co_{18.21}/MgO-0.75Al_2O_3$ , as well as the  $Ni_{25.38}Co_{18.21}/MgO-0.75Al_2O_3$  after on stream for 20 h are shown in Fig. 6. The characteristic diffraction peaks of  $Ni^0$  phase are clearly observed in the patterns of first three samples, and the peaks of  $Ni^0/Co^0$  phases are found in the patterns of the last two ones at  $2\theta = 44.5^\circ$ ,  $51.8^\circ$  and  $76.4^\circ$ , which are ascribed to the planes (111), (200) and (220) [42]. Overlapping of the diffraction peaks of  $Ni^0$  (JCPDS no. 87-0712) and  $Co^0$  (JCPDS no. 15-0806) phases impeded their separate identification in the bimetallic catalyst samples. The peaks ascribed to NiO (JCPDS no. 73-1523) phase at  $2\theta = 43.1^\circ$  and  $62.8^\circ$  were clearly observed in the pattern of  $Ni_{46.63}/MgO$ , which was ascribed to the oxidation of  $Ni^0$  to NiO in analysis [43]. Importantly, the patterns of the used  $Ni_{25.38}Co_{18.21}/MgO-0.75Al_2O_3$  are virtually identical to those of the fresh one, also indicating the stability of the catalyst on stream.

To reveal the states of surface Co and Ni in the catalysts, the reduced catalysts were characterized by X-ray photoelectron spectra (XPS). As exhibited in the wide scan XPS spectra of the samples (Fig. 7A), distinct peaks of Ni 2p, Mg 1s, Co 2p, O 1s, C 1s and Al 2p were observed clearly. The XPS spectrum of the used  $Ni_{25.38}Co_{18.21}/MgO-0.75Al_2O_3$  was almost identical to that of the fresh one, further confirming its stability of the catalyst in the catalytic run. The fitted Ni 2p XPS spectra for the catalysts corresponding to

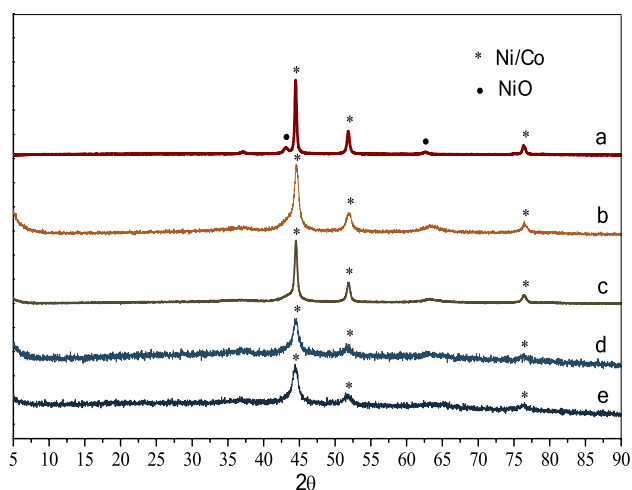


**Fig. 6** XRD patterns of catalyst samples (a)  $Ni_{46.63}/MgO$ ; (b)  $Ni_{40.85}/Al_2O_3$ ; (c)  $Ni_{43.55}/MgO-0.5Al_2O_3$ ; (d)  $Ni_{25.38}Co_{18.21}/MgO-0.75Al_2O_3$ ; (e)  $Ni_{25.38}Co_{18.21}/MgO-0.75Al_2O_3$  (used)

the binding energies between 845 and 895 eV, including the peaks Ni 2p<sub>1/2</sub> and Ni 2p<sub>3/2</sub> for nickel, are shown in Fig. 7B. The Ni 2p<sub>3/2</sub> binding energies of 852.41 eV and 852.75 eV correspond to the metallic nickel [44, 45] in the samples of  $Ni_{46.63}/MgO$  and  $Ni_{40.85}/Al_2O_3$ , respectively, whereas the binding energy of about 855.1 eV is assigned to the  $Ni^{2+}$  species [46] in both the samples. It should be noted that the  $Ni^{2+}$  species found in all the catalyst samples is due to the oxidation of  $Ni^0$  species during analysis. The Ni 2p<sub>3/2</sub> binding energy of  $Ni^0$  in  $Ni_{46.63}/MgO$  is lower than that in  $Ni_{40.85}/Al_2O_3$  due to more electron transfer from MgO to  $Ni^0$  species [47], indicating the stronger metal-support interaction between  $Ni^0$  species and MgO than that between  $Ni^0$  species and  $Al_2O_3$ . In the mixed oxide supported catalyst  $Ni_{43.55}/MgO-0.5Al_2O_3$ , the binding energy of Ni 2p<sub>3/2</sub> for  $Ni^0$  is 852.59 eV between the ones in  $Ni_{46.63}/MgO$  and  $Ni_{40.85}/Al_2O_3$ .

The binding energy of Ni 2p<sub>3/2</sub> for  $Ni^0$  in the catalyst  $Ni_{25.38}Co_{18.21}/MgO-0.75Al_2O_3$  was 853.72 eV, much bigger than that in the  $Ni_{43.55}/MgO-0.5Al_2O_3$ , suggesting the formation of Ni/Co alloy. This result seems contradictory, because the electronegativity of  $Ni^0$  is greater than that of  $Co^0$ , upon the Ni/Co alloy formed, more electrons of  $Co^0$  will flow to  $Ni^0$ , leading to lower binding energy of Ni 2p<sub>3/2</sub> for  $Ni^0$ . However, the shifting of Ni 2p<sub>3/2</sub> binding energy for  $Ni^0$  in the Ni/Co alloy to higher energy rather than lower energy was due to the fact that  $Co^0$  species were almost completely oxidized to cobalt oxides during the analysis process as revealed in Fig. 7C, which led to more electrons transfer from  $Ni^0$  to cobalt oxides, resulting in bigger binding energy of Ni 2p<sub>3/2</sub> for  $Ni^0$  in the catalyst. The formation of Ni/Co alloy endowed a synergy effect between nickel and cobalt in the catalytic reaction, which enhanced the selectivity towards primary amines in the hydrogenation of aliphatic nitriles [29, 42, 48]. The fitted Co 2p XPS spectra for the reduced catalysts  $Co_{43.65}/MgO-0.5Al_2O_3$  and  $Ni_{25.38}Co_{18.21}/MgO-0.75Al_2O_3$  were shown in Fig. 7C. The Co 2p<sub>3/2</sub> binding energy of 777.6 eV corresponds to the  $Co^0$  species, and the Co 2p<sub>3/2</sub> binding energies of 779.6 eV and 780.4 eV are attributed to the  $Co^{2+}$  and  $Co^{3+}$  oxide species in the catalysts  $Co_{43.65}/MgO-0.5Al_2O_3$  and  $Ni_{25.38}Co_{18.21}/MgO-0.75Al_2O_3$  [49–51]. The results indicated that the  $Co^0$  species in the reduced catalysts were very easily oxidized, so the catalysts must be reduced in situ in application.

The textural properties of the reduced catalysts  $Ni_{46.63}/MgO$ ,  $Ni_{40.85}/Al_2O_3$ ,  $Ni_{43.55}/MgO-0.5Al_2O_3$ ,  $Ni_{25.38}Co_{18.21}/MgO-0.75Al_2O_3$ , as well as the used  $Ni_{25.38}Co_{18.21}/MgO-0.75Al_2O_3$  were determined by  $N_2$  adsorption–desorption analysis. As shown in Fig. 8, all the samples showed standard type IV isotherms, indicating the existence of mesopores in the catalysts. Besides, the presence of hysteric loops similar to the type H4 is indicative of slit-like pores [52]. The similarity of the isotherms of the samples

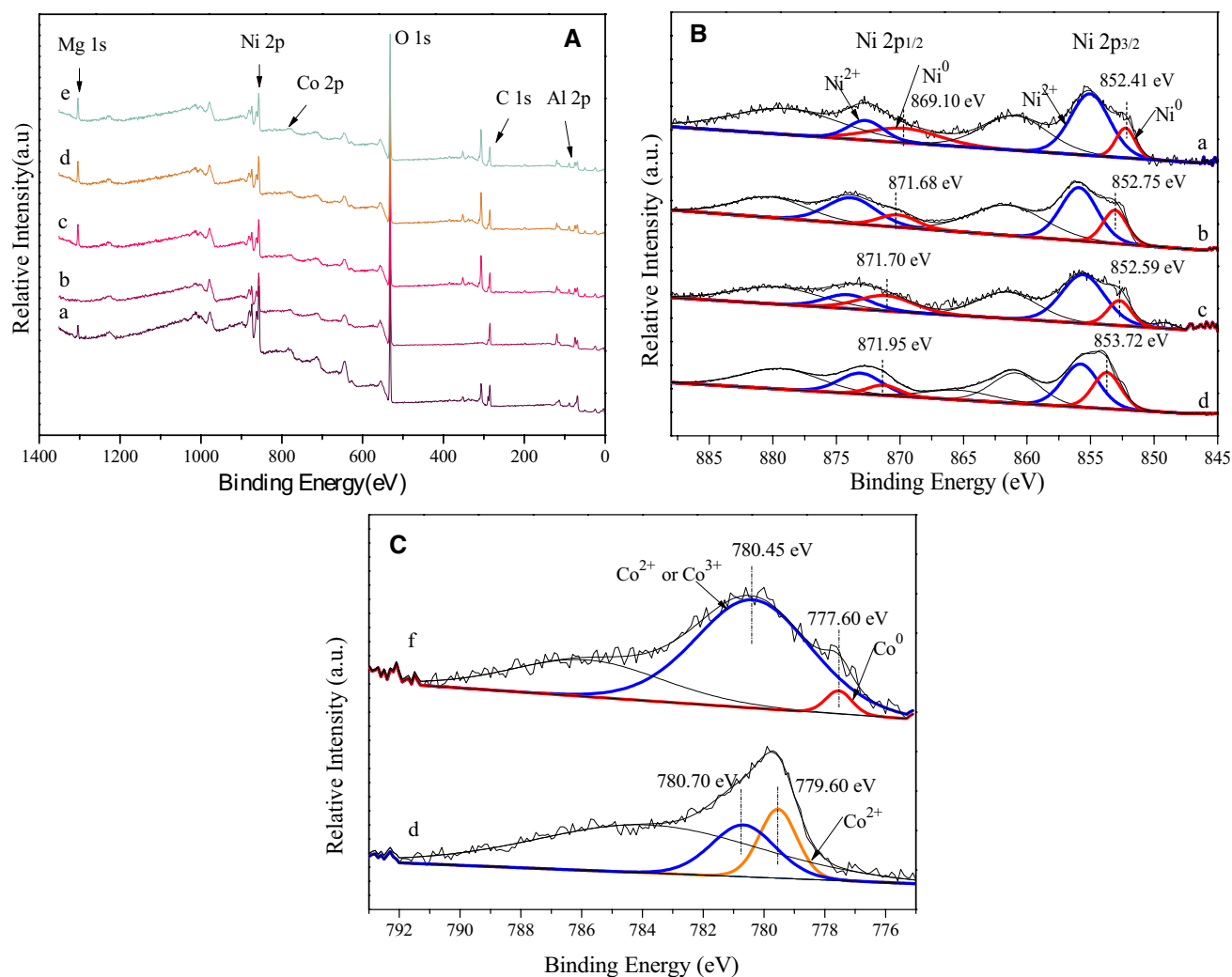


**Fig. 7** The wide scan XPS spectra (A), Ni 2p XPS spectra of samples (B) and Co $2p_{3/2}$  XPS spectra (C) of the samples (a) Ni $_{46.63}$ /MgO; (b) Ni $_{40.85}$ /Al $_2$ O $_3$ ; (c) Ni $_{43.55}$ /MgO–0.5Al $_2$ O $_3$ ; (d) Ni $_{25.38}$ Co $_{18.21}$ /MgO–

0.75Al $_2$ O $_3$ ; (e) Ni $_{25.38}$ Co $_{18.21}$ /MgO–0.75Al $_2$ O $_3$  (used); (f) Co $_{43.65}$ /MgO–0.5Al $_2$ O $_3$

of the fresh and used Ni $_{25.38}$ Co $_{18.21}$ /MgO–0.75Al $_2$ O $_3$  again confirmed the stability of the catalyst in catalytic run.

The specific surface areas and the range of the pore structural parameters of the catalyst samples are presented in Table 2. As seen, the surface areas of the catalysts were related to the supports. For the three mono nickel catalysts, the surface area, pore volume, and pore diameter are all in the order of Ni $_{40.85}$ /Al $_2$ O $_3$  > Ni $_{43.55}$ /MgO–0.5Al $_2$ O $_3$  > Ni $_{46.63}$ /MgO. The bimetallic catalyst Ni $_{25.38}$ Co $_{18.21}$ /MgO–0.75Al $_2$ O $_3$  showed higher surface area, pore volume, and pore diameter compared to Ni $_{43.55}$ /MgO–0.5Al $_2$ O $_3$ . It also had bigger surface area and pore volume than Ni $_{40.85}$ /Al $_2$ O $_3$ . The big surface area of Ni $_{25.38}$ Co $_{18.21}$ /MgO–0.75Al $_2$ O $_3$  could be ascribed to the doping of nickel with cobalt leading to decrease in the sizes of metal particles as disclosed by

TEM, which endowed this catalyst good performances in the hydrogenation of VN to AA.

After the catalyst Ni $_{25.38}$ Co $_{18.21}$ /MgO–0.75Al $_2$ O $_3$  was on stream for 20 h, both the surface area and the pore volume decreased slightly as shown in Table 2, which could be ascribed to the slight deposition of carbon and nonvolatile amine condensates on the pores of the catalyst. On the contrary, the mean pore diameter of the used catalyst increased slightly compared to that of the fresh one because of the deposition of substances on the small pores, leading to the shift in the pore size distributions to large ones. The deposition of some nonvolatile substances on the pores of the catalyst impeded reactants access to the active centers of the catalyst in the catalytic run, leading to a decrease in the yield of AA as shown in Fig. 5.

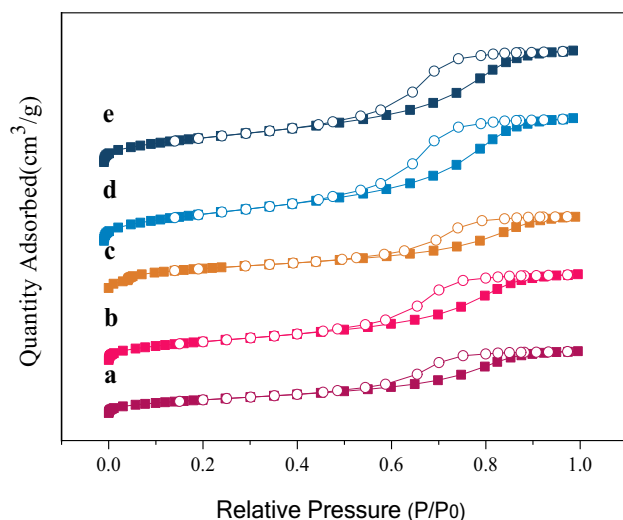


**Fig. 8** Adsorption–desorption isotherms of the catalyst samples (a)  $\text{Ni}_{46.63}/\text{MgO}$ ; (b)  $\text{Ni}_{40.85}/\text{Al}_2\text{O}_3$ ; (c)  $\text{Ni}_{43.55}/\text{MgO}-0.5\text{Al}_2\text{O}_3$ ; (d)  $\text{Ni}_{25.38}\text{Co}_{18.21}/\text{MgO}-0.75\text{Al}_2\text{O}_3$ ; (e)  $\text{Ni}_{25.38}\text{Co}_{18.21}/\text{MgO}-0.75\text{Al}_2\text{O}_3$  (used)

The transmission electron micrograph (TEM) of the catalysts  $\text{Ni}_{43.55}/\text{MgO}-0.5\text{Al}_2\text{O}_3$  and  $\text{Ni}_{25.38}\text{Co}_{18.21}/\text{MgO}-0.75\text{Al}_2\text{O}_3$  were taken finally. As shown in Fig. 9, nickel and nickel–cobalt nanoparticles are dispersed on  $\text{MgO}-\text{Al}_2\text{O}_3$  support with diameters of 22.45–29.75 nm (Fig. 9a and c) and 11.65–19.89 nm (Fig. 9b and d), respectively. The results revealed that the doping of nickel with cobalt led to decrease in average sizes and uniform dispersion of Ni/Co nanoparticles, which were the main reasons for the good performances of  $\text{Ni}_{25.38}\text{Co}_{18.21}/\text{MgO}-0.75\text{Al}_2\text{O}_3$  compared to the other ones in the

hydrogenation of VN to AA. In addition, HRTEM images of the  $\text{Ni}_{25.38}\text{Co}_{18.21}/\text{MgO}-0.75\text{Al}_2\text{O}_3$  sample clearly manifested lattice fringes of 0.203 nm (Fig. 9e), which could be assigned to the 111 crystal plane of Ni and Co or Ni/Co alloy [10, 53, 54].

The EDX elemental mapping revealed that the areas of nickel and cobalt species overlapped well (Fig. 9f–i), also indicating the formation of Ni/Co alloy. Besides, magnesium and aluminum also located in the same zone, which confirmed the perfect mixing of  $\text{Al}_2\text{O}_3$  and  $\text{MgO}$  in the catalyst, affording good dispersion of active centers on the support.

## 4 Conclusion

The screened bimetallic catalyst  $\text{Ni}_{25.38}\text{Co}_{18.21}/\text{MgO}-0.75\text{Al}_2\text{O}_3$  showed good catalytic performances in the hydrogenation of VN as well as other low carbon aliphatic nitriles to their corresponding primary amines under atmospheric pressure in the presence of ammonia in a fixed bed reactor. The conversion of VN reached 100% with a AA yield of 70.8% and a total yield of AA and DAA of 96.7% under the optimal conditions. The catalyst also showed good stability and ease of regeneration. The good performances of the catalyst could be ascribed to the large surface area of the catalyst, uniform and fine dispersion of metal nanoparticles on the mixed oxide support, and formation of Ni/Co alloy with synergy effect between the two metals in the reduced  $\text{Ni}_{25.38}\text{Co}_{18.21}/\text{MgO}-0.75\text{Al}_2\text{O}_3$ .

**Table 2** Textural properties of catalysts

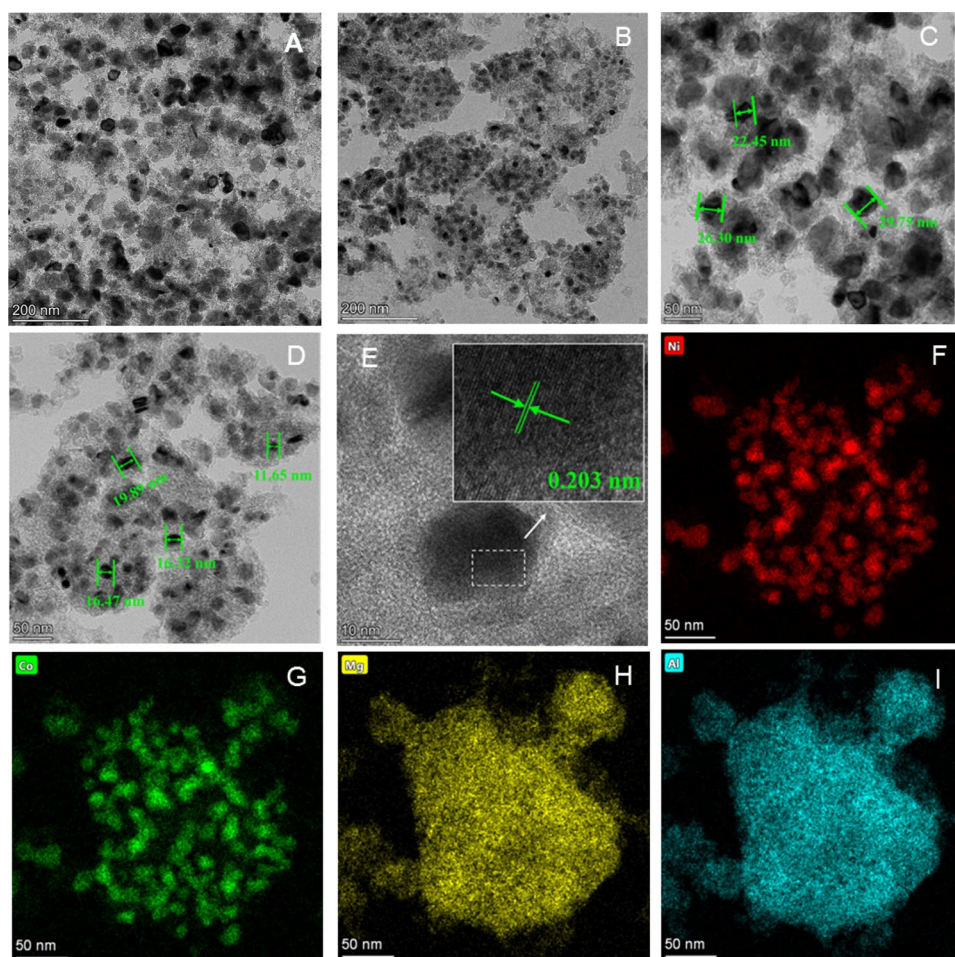
| Entry | Catalyst   | $S_{\text{BET}}^{\text{a}}$ ( $\text{m}^2/\text{g}$ ) | $V^{\text{b}}$ ( $\text{cm}^3/\text{g}$ ) | $d_p^{\text{c}}$ (nm) |
|-------|--|---|---|-----------------------|
| 1     | $\text{Ni}_{46.63}/\text{MgO}$   | 98.21   | 0.13                                      | 2.30                  |
| 2     | $\text{Ni}_{40.85}/\text{Al}_2\text{O}_3$  | 156.70  | 0.30                                      | 4.91                  |
| 3     | $\text{Ni}_{43.55}/\text{MgO}-0.5\text{Al}_2\text{O}_3$                          | 123.26  | 0.22                                      | 4.62                  |
| 4     | $\text{Ni}_{25.38}\text{Co}_{18.21}/\text{MgO}-0.75\text{Al}_2\text{O}_3$        | 168.10  | 0.33                                      | 4.85                  |
| 5     | $\text{Ni}_{25.38}\text{Co}_{18.21}/\text{MgO}-0.75\text{Al}_2\text{O}_3$ (used) | 152.50  | 0.27                                      | 5.22                  |

<sup>a</sup>BET surface area

<sup>b</sup>BJH cumulative desorption pore volume

<sup>c</sup>Mean pore diameter =  $4V/S_{\text{BET}}$

**Fig. 9** TEM images of  $\text{Ni}_{43.55}/\text{MgO}-0.5\text{Al}_2\text{O}_3$  (a, c),  $\text{Ni}_{25.38}\text{Co}_{18.21}/\text{MgO}-0.75\text{Al}_2\text{O}_3$  (b, d, e), and corresponding element mappings of  $\text{Ni}_{25.38}\text{Co}_{18.21}/\text{MgO}-0.75\text{Al}_2\text{O}_3$  (f–i)



**Acknowledgements** We thank the financial support from the National Natural Science Foundation of China (Grant No. 21476057), the Central Government Guides Local Science and Technology Development Project (Grant No. 206Z4001G) and the Natural Science Foundation of Hebei Province of China (Grant No. B2016202393).

### Compliance with Ethical Standards

**Conflict of interest** The authors declare that they have no conflict of interest.

### References

- Lawrence SA (2004) Amines: synthesis, properties and applications. Cambridge University Press, Cambridge
- Pohlki F, Doye S (2003) Chem Soc Rev 32:104
- Ricci A (2008) Amino group chemistry: from synthesis to the life sciences. Wiley-VCH, Weinheim
- Gallardo-Donaire J, Hermsen M, Wysocki J, Ernst M, Rominger F, Trapp O, Hashmi AS, Schafer A, Comba P, Schaub T (2018) J Am Chem Soc 140:355
- Liang G, Wang A, Li L, Xu G, Yan N, Zhang T (2017) Angew Chem Int Ed 129:3096
- Aubin Y, Fischmeister C, Thomas CM, Renaud J (2010) Chem Soc Rev 39:4130
- Gunanathan C, Milstein D (2008) Angew Chem Int Ed 120:8789
- Das K, Shibuya R, Nakahara Y, Germain N, Ohshima T, Mashima K (2012) Angew Chem Int Ed 124:154
- Pingen D, Diebolt O, Vogt D (2013) ChemCatChem 5:2905
- Qu Y, Xu G, Yang J, Zhang Z (2020) Appl Catal A Gen 59011:7311
- Peng Y, Geng Z, Zhao S, Wang L, Li H, Wang X, Zheng X, Zhu J, Li Z, Si R, Zeng J (2018) Nano Lett 18:3785
- Zhang G, Tang F, Wang X, An P, Wang L, Liu YN (2020) ACS Sustain Chem Eng 8:6118
- Lévay K, Hegedűs L (2019) Curr Org Chem 23:1881
- Blondiaux E, Cantat T (2014) Chem Commun 50:9349
- Shimizu K-i, Kanno S, Kon K, Hakim Siddiki SMA, Tanaka H, Sakata Y (2014) Catal Today 232:134
- Roose P, Eller K, Henkes E, Roszbacher R, Höke H (2015) Amines, aliphatic. Wiley-VCH, Weinheim
- Zhang Y, Zhang Y, Feng C, Qiu C, Wen Y, Zhao J (2009) Catal Commun 10:1454
- Zhang D, Zhang Y, Wen Y, Hou K, Zhao J (2011) Chem Eng Res Des 89:2147
- Zhang Y, Wei T, Pian Y, Zhao J (2013) Appl Catal A Gen 467:154
- Hu Y, Jin S, Zhang Z, Zhang L, Deng J, Zhang H (2014) Catal Commun 54:45
- Dai H, Guan H (2018) ACS Catal 8:9125

22. Adam R, Bheeter CB, Cabrero-Antonino JR, Junge K, Jackstell R, Beller M (2017) *ChemSusChem* 10:842
23. Tokmic K, Jackson BJ, Salazar A, Woods TJ, Fout AR (2017) *J Am Chem Soc* 139:13554
24. Wang J, Tang Q, Jin S, Wang Y, Yuan Z, Chi Q, Zhang Z (2020) *New J Chem* 44:549
25. Hegedus L, Máthé T (2005) *Appl Catal A Gen* 296:209
26. Segobia DJ, Trasarti AF, Apesteguía CR (2012) *Appl Catal A Gen* 445–446:69
27. Huang Y, Adeeva V, Sachtler WMH (2000) *Appl Catal A Gen* 196:73
28. Rode CV, Arai M, Shirai M, Nishiyama Y (1997) *Appl Catal A Gen* 148:405
29. Coq B, Tichit D, Ribet S (2000) *J Catal* 189:117
30. Huang Y, Sachtler WMH (1999) *J Catal* 188:215
31. Hao Y, Li M, Cárdenas-Lizana F, Keane MA (2016) *Catal Struct React* 1:132
32. Segobia DJ, Trasarti AF, Apesteguía CR (2014) *Catal Struct React* 4:4075
33. Saad F, Comparot JD, Brahmi R, Bensitel M, Pirault-Roy L (2017) *Appl Catal A Gen* 544:1
34. Gluhoi AC, Mărginean P, Stănescu U (2005) *Appl Catal A Gen* 294:208
35. Verhaak MJFM, Dillen AJ, Geus JW (1994) *Catal Lett* 26:37
36. Chen H, Xue M, Hu S, Shen J (2012) *Chem Eng J* 181–182:677
37. Yadav GD, Kharkara MR (1995) *Appl Catal A Gen* 126:115
38. Arai M, Ebina T, Shirai M (1999) *Appl Surf Sci* 148(3–4):155
39. Braos-García P, García-Sancho C, Infantes-Molina A, Rodríguez-Castellón E, Jiménez-López A (2010) *Appl Catal A Gen* 381:132
40. Liu C, Li X, Wang T (2015) *RSC Adv* 5:57277
41. Gomez S, Peters JA, Maschmeyer T (2002) *Adv Synth Catal* 344:1037
42. Santamaria L, Lopez G, Arregi A, Artetxe M, Amutio M, Bilbao J, Olazar M (2020) *J Ind Eng Chem* 91:167
43. Qiu Y, Huang H, Song W, Gan Y, Wang K, Zhang J, Xia Y, Liang C, He X, Zhang W (2020) *J Alloys Compd* 834:155111
44. Sciortino L, Giannici F, Martorana A, Ruggirello AM, Liveri VT, Portale G, Casaletto MP, Longo A (2011) *J Phys Chem C* 115:6360
45. Aldana-González J, Romero-Romo M, Robles-Peralta J, Morales-Gil P, Palacios-González E, Ramírez-Silva MT, Mostany J, Palomar-Pardavé M (2018) *Electrochim Acta* 276:417
46. Zhang S, Huang BS, Shi C, Xu Q, Zhu Y (2020) *Colloids Surf A* 605:125243
47. Gao T, Chen J, Fang W, Cao Q, Su W, Dumeignil F (2018) *J Catal* 368:53
48. Lozano-Blanco G, Adamczyk AJ (2019) *Surf Sci* 688:31
49. Sarnecki A, Adamski P, Albrecht A, Komorowska A, Nadziejko M, Moszyński D (2018) *Vacuum* 155:434
50. Łojewska J, Makowski WA, Tyszewski T, Dziembaj R (2001) *Catal Today* 69:409
51. Zhao B, Liu P, Li S, Shi H, Jia X, Wang Q, Yang F, Song Z, Guo C, Hu J, Chen Z, Yan X, Ma X (2020) *Appl Catal B Environ* 278:119307
52. Lowell S, Shields JE, Thommes M, Thomas MA (2004) *Characterization of porous solids and powders: surface area, pore size and density*. Springer Science+Business Media, New York
53. Zhang F, Zhao C, Chen S, Li H, Yang H, Zhang XM (2017) *J Catal* 348:212
54. Wang Z, Wang C, Chen S, Liu Y (2014) *Int J Hydrog Energy* 39:5644

**Publisher's Note** Springer Nature remains neutral with regard to jurisdictional claims in published maps and institutional affiliations.

## Authors and Affiliations

Dongxu Shi<sup>1</sup> · He Zhu<sup>1</sup> · Yaping Han<sup>1</sup> · Yuecheng Zhang<sup>1,3</sup> · Jiquan Zhao<sup>1,2</sup>

<sup>1</sup> School of Chemical Engineering and Technology, Hebei University of Technology, Tianjin 300131, China

<sup>2</sup> Hebei Provincial Key Laboratory of Green Chemical Technology and High Efficient Energy Saving, Tianjin 300131, China

<sup>3</sup> Tianjin Key Laboratory of Chemical Process Safety, Tianjin 300131, China